Editors' Suggestion

Unconventional Superconductivity in Systems with Annular Fermi Surfaces: Application to Rhombohedral Trilayer Graphene

Areg Ghazaryan,[1,*] Tobias Holder,[2,*] Maksym Serbyn,[1] and Erez Berg[2]
[1]IST Austria, Am Campus 1, 3400 Klosterneuburg, Austria
[2]Department of Condensed Matter Physics, Weizmann Institute of Science, Rehovot 76100, Israel

(Received 7 September 2021; accepted 12 November 2021; published 9 December 2021)

We show that in a two-dimensional electron gas with an annular Fermi surface, long-range Coulomb interactions can lead to unconventional superconductivity by the Kohn-Luttinger mechanism. Superconductivity is strongly enhanced when the inner and outer Fermi surfaces are close to each other. The most prevalent state has chiral p-wave symmetry, but d-wave and extended s-wave pairing are also possible. We discuss these results in the context of rhombohedral trilayer graphene, where superconductivity was recently discovered in regimes where the normal state has an annular Fermi surface. Using realistic parameters, our mechanism can account for the order of magnitude of T_c, as well as its trends as a function of electron density and perpendicular displacement field. Moreover, it naturally explains some of the outstanding puzzles in this material, that include the weak temperature dependence of the resistivity above T_c, and the proximity of spin singlet superconductivity to the ferromagnetic phase.

DOI: 10.1103/PhysRevLett.127.247001

Introduction.—Graphene based two-dimensional materials offer a unique platform to study correlated electron phenomena with an unprecedented level of control [1–10]. Among these, rhombohedral trilayer graphene (RTG) [11–14] has recently been shown to exhibit a rich phase diagram, including several spin and valley polarized states, tunable by varying the electron density and perpendicular electric field [15]. Most strikingly, two distinct superconducting phases were discovered in different regions of the phase diagram [16]. The emergence of superconductivity in this ultrapure and tunable system calls for a theoretical understanding, potentially shedding light on long-standing problems in condensed matter physics and opening the way to future applications.

In this Letter, we examine the key experimental facts about superconductivity in RTG, and identify two puzzles that seem difficult to reconcile with conventional, phonon-mediated superconductivity. We argue that these puzzles can be resolved if one assumes an unconventional mechanism for superconductivity [17]. Interestingly, superconductivity is found in regimes where the normal-state Fermi surface (FS) has an annular shape, with an inner electron pocket and an outer hole pocket. We show that an annular FS is beneficial for an electronic mechanism for superconductivity [18–24], driven by repulsive Coulomb interactions. Using a microscopic model for RTG with realistic parameters, we find that the most likely candidate for the superconducting order parameter is a chiral p wave, followed by extended s wave [25].

Superconductivity in RTG.—The band structure of RTG [11,12] exhibits strong peaks in the density of states, tunable by a perpendicular electric field, at finite density of electron or holes. Therefore, upon doping RTG undergoes a cascade of phase transitions between different spin and valley polarized phases [15], reminiscent of the observations in twisted bilayer graphene [26,27], despite the absence of a moiré lattice in RTG.

Recently, two superconducting phases were discovered in the hole-doped side, labeled by SC1 and SC2 [16]. SC1 is found within the flavor-symmetric phase. Its maximum critical temperature is $T_{c1} \approx 100$ mK. SC2 occurs within a fully spin-polarized, valley-unpolarized half-metal, with a $T_{c2} \lesssim 50$ mK. In both phases, the coherence length is shorter than the mean free path, placing them in the clean limit. The in-plane critical magnetic field of SC1 is consistent with the Pauli limit [28,29], while for SC2 the critical field exceeds the limit by an order of magnitude.

It has been proposed [30] that RTG is a "conventional" phonon-driven superconductor, with an s-wave-like gap wave function within each valley. We point out two difficulties with this scenario. First, coupling to acoustic phonon modes should lead to a linear dependence of the resistivity for $T \gtrsim \Theta_{\mathrm{BG}}/4$, where $\Theta_{\mathrm{BG}} \approx 40$ K is the Bloch-Grüneisen temperature at the density range of SC1. However, the resistance of RTG above SC1 is nearly temperature independent up to $T = 20$ K [16]. This is unlike many conventional superconductors, where estimates for the dimensionless electron-phonon coupling from T_c and from the slope of the resistivity vs T typically agree [31]. Second, SC1 emerges out of a spin- and valley-unpolarized normal state [15,16]. As explained below, SC1 can be either spin singlet or triplet, and one expects the intervalley exchange coupling J_H to determine which one is realized. Experimentally, SC1 is spin singlet, which implies

$J_H < 0$ for an s-wave-like gap function. This is in apparent contradiction with the presence of a spin polarized ferromagnetic state nearby in the phase diagram, that requires $J_H > 0$ [32].We argue that both of these puzzles are resolved for an all-electronic mechanism that leads to unconventional superconductivity.

Model.—The Hamiltonian used to describe rhombohedral trilayer graphene reads

$$\hat{H} = \hat{H}_0 + \hat{H}_C, \tag{1}$$

where $\hat{H}_0 = \sum_{\boldsymbol{k},\tau,s} \Psi^\dagger_{\boldsymbol{k}\tau s} h_{\boldsymbol{k}\tau} \Psi_{\boldsymbol{k}\tau s}$ is the single-particle part [12]. $h_{\boldsymbol{k}\tau}$ is a 6×6 matrix in the basis $(A_1, B_1, A_2, B_2, A_3, B_3)$, corresponding to the A, B sublattices of layers 1,2,3 [Fig. 1(a)] that is written explicitly in the Supplemental Material [33]. The valley and spin indices are denoted by τ and s, respectively. $\Psi^\dagger_{\boldsymbol{k}\tau s}$ is a spinor containing the operators $\psi^\dagger_{\boldsymbol{k},\ell,\sigma,\tau,s}$, that create an electron with momentum $\boldsymbol{k}$, at layer $\ell = 1, 2, 3$ and sublattice $\sigma = A, B$. The Coulomb interaction between Fourier component of the density $\rho_{\boldsymbol{q}} = \sum_{\boldsymbol{k}\tau s} \Psi^\dagger_{\boldsymbol{k}\tau s} \Psi_{\boldsymbol{k}+\boldsymbol{q}\tau s}$ is given by

$$\hat{H}_C = \frac{1}{2L^2} \sum_{\boldsymbol{q}} V_{0,\boldsymbol{q}} \rho_{\boldsymbol{q}} \rho_{-\boldsymbol{q}}, \tag{2}$$

where $V_{0,\boldsymbol{q}} = (2\pi e^2/\epsilon q)\tanh(qd)$ is the Coulomb potential screened by two metallic gates at distance d above and below the RTG, ϵ is the dielectric constant, and L^2 is the area of the system.

Near the Fermi level, the band structure of $h_{\boldsymbol{k}\tau}$ consists of a conduction and a valence band separated by a gap $2\Delta_1$, proportional to the perpendicular displacement field. Δ_1 and the carrier density n_e, controlled experimentally by gate voltages, tune the system between different phases.

We project the Hamiltonian onto the valence band, where SC1 and SC2 occur. This amounts to substituting $\rho_{\boldsymbol{q}}$ by $\tilde{\rho}_{\boldsymbol{q}} = \sum_{\boldsymbol{k},\tau,s} \Lambda_{\boldsymbol{k},\boldsymbol{q},\tau} c^\dagger_{\boldsymbol{k},\tau,s} c_{\boldsymbol{k}+\boldsymbol{q},\tau,s}$, where $c^\dagger_{\boldsymbol{k},\tau,s}$ creates an electron at momentum $\boldsymbol{k}$ in the valence band in valley τ and spin s, and $\Lambda_{\boldsymbol{k},\boldsymbol{q},\tau} = \langle u_{\boldsymbol{k},\tau} | u_{\boldsymbol{k}+\boldsymbol{q},\tau} \rangle$ is an overlap between Bloch wave functions of the valence band, $|u_{\boldsymbol{k},\tau}\rangle$.

We investigate superconductivity within a purely electronic mechanism, driven by the Coulomb interaction. Within this mechanism [18,20], pairing is mediated by particle-hole fluctuations at a broad range of energies. The effective interaction after screening by such fluctuations depends weakly on frequency, and will be treated as instantaneous. Within the random phase approximation (RPA), this interaction is given by

$$V_{\boldsymbol{q}} = \frac{V_{0,\boldsymbol{q}}}{1 + \Pi_{0,\boldsymbol{q}} V_{0,\boldsymbol{q}}}, \tag{3}$$

where $\Pi_{0,\boldsymbol{q}} = N \sum_{\boldsymbol{k}} |\Lambda_{\boldsymbol{k},\boldsymbol{q},\tau}|^2 \{[f(\varepsilon_{\boldsymbol{k},\tau}) - f(\varepsilon_{\boldsymbol{k}+\boldsymbol{q},\tau})]/(\varepsilon_{\boldsymbol{k}+\boldsymbol{q},\tau} - \varepsilon_{\boldsymbol{k},\tau})\}$ is the static polarization function, with $\varepsilon_{\boldsymbol{k},\tau}$ being the dispersion of the valence band in valley τ. $f(\varepsilon)$ is the Fermi function. $N = 4$ is the number of spin and valley flavors. Note that $\Pi_{0,\boldsymbol{q}}$ is independent of τ due to time reversal symmetry.

The RPA interaction Hamiltonian is given by $\hat{H}_{\mathrm{RPA}} = (1/2L^2)\sum_{\boldsymbol{q}} V_{\boldsymbol{q}} \tilde{\rho}_{\boldsymbol{q}} \tilde{\rho}_{-\boldsymbol{q}}$. The superconducting T_c is found by solving the linearized BCS gap equation using Eq. (3) as the pairing interaction [33]. The gap equation reads

$$\Delta_{\boldsymbol{k}} = -\log\left(\frac{W}{T_c}\right) \int_{\mathrm{FS}} \frac{dk'_{\parallel}}{(2\pi)^2 v_{\boldsymbol{k}'}} V_{\boldsymbol{k}-\boldsymbol{k}'} |\Lambda_{\boldsymbol{k},\boldsymbol{k}'-\boldsymbol{k},+1}|^2 \Delta_{\boldsymbol{k}'}, \tag{4}$$

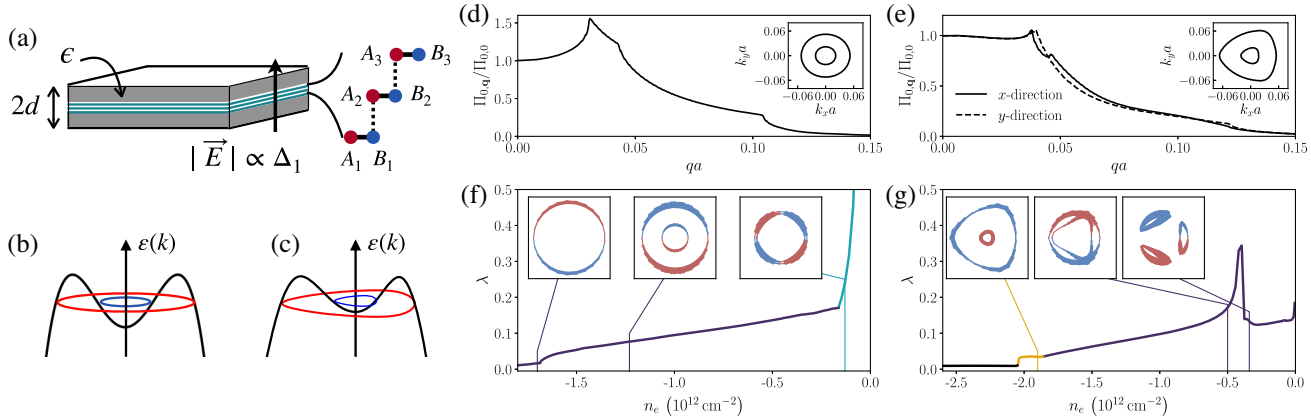

FIG. 1. (a) RTG placed between two metallic gates at distance d away, and encapsulated by an insulator with dielectric constant ϵ. (b), (c) Band structure and FS of the simplified circularly symmetric model and the realistic model, respectively. (d),(e) The polarization function $\Pi_{0,\boldsymbol{q}}$ within the simplified and realistic models, at density $n_e = -1.19 \times 10^{12}$ and $n_e = -1.67 \times 10^{12}$ cm^{-2}, respectively. (f),(g) SC dimensionless coupling constant λ vs density in the two models, colored for p wave (purple), extended s wave (yellow), and d wave (cyan). The inset shows the solution of the linearized gap equation along the FS at certain values of n_e. Red (blue) color represents positive (negative) $\Delta_{\boldsymbol{k}}$. We used $\epsilon = 4$ and $d = 36.9$ nm in (f)–(g) and $\Delta_1 = 20$ meV in (e),(g).

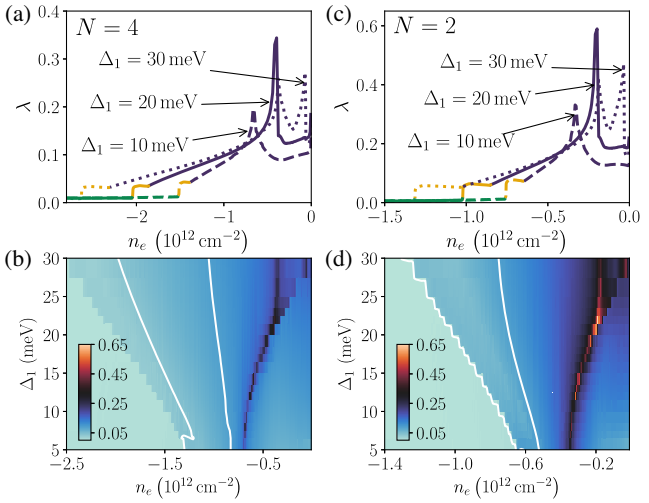

FIG. 2. (a),(b) Coupling constant λ as a function of density and displacement field Δ_1 for the unpolarized state, $N = 4$. (c),(d) Same as (a),(b) assuming the spin polarization, $N = 2$. The color coding in (a),(c) is identical to Fig. 1. The white contours in (b),(d) indicate $\lambda = 0.05$, 0.1.

where $\Delta_{\boldsymbol{k}}$ is the SC order parameter at a point $\boldsymbol{k}$ on the FS in valley $\tau = +1$, $v_{\boldsymbol{k}}$ is the magnitude of the Fermi velocity at that point, and W is an upper cutoff of the order of the Fermi energy. The integration is taken over all FSs. The largest eigenvalue λ of the linear operator $\mathcal{M}$ defined by $\mathcal{M}\Delta_{\boldsymbol{k}} = -\int dk'_{\parallel}/[(2\pi)^2 v_{\boldsymbol{k}'}] V_{\boldsymbol{k}-\boldsymbol{k}'} |\Lambda_{\boldsymbol{k},\boldsymbol{k}'-\boldsymbol{k},+1}|^2 \Delta_{\boldsymbol{k}'}$, yields $T_c = We^{-1/\lambda}$.

Kohn-Luttinger mechanism: Idealized model.—Since $V_{\boldsymbol{q}} > 0$ for all $\boldsymbol{q}$, a solution $\Delta_{\boldsymbol{k}}$ of Eq. (4) must change the sign across the FS. Therefore, the solution typically has a non s-wave symmetry, depending on the structure of $\Pi_{0,\boldsymbol{q}}$. For a single parabolic band in two dimensions, $\Pi_{0,\boldsymbol{q}}$ is constant up to $q = 2k_F$, and Eq. (4) has no solution [34]. In the case of two subbands with different Fermi momenta, the total polarization function is no longer a constant for momenta smaller than $2k_F$ of the outer FS, yielding nontrivial solutions [23,24]. In RTG, both SC1 and SC2 occur in regions where the normal state exhibits an annular FS, where the inner and outer Fermi surfaces have opposite Fermi velocities. As we demonstrate, such a dispersion is favorable for superconductivity.

We begin with a simplified model where the dispersion is approximated as $\varepsilon_{\boldsymbol{k}} = -\varepsilon_0(k^2/k_0^2 - 1)^2 - \mu$, characterized by an energy scale ε_0 and a momentum scale k_0, Fig. 1(b). Moreover, we approximate $\Lambda_{\boldsymbol{k},\boldsymbol{q},\tau} = 1$. Because of the rotational symmetry of this model, $\Pi_{0,\boldsymbol{q}}$ can be computed analytically [33]. $\Pi_{0,\boldsymbol{q}}$ exhibits singularities for $2k_{F1}$, $2k_{F2}$, and $k_{F1} - k_{F2}$, where $k_{F1,2} = k_0\sqrt{1 \pm \sqrt{-\mu/\varepsilon_0}}$ are the momenta of the outer and inner FS, respectively, see Fig. 1(d).

The result for λ as a function of electron density is shown in Fig. 1(f). At large hole densities where the inner pocket disappears, λ is nearly zero. λ increases discontinuously once the inner pocket appears (around $n_e = -1.7 \times 10^{12}$ cm^{-2}). The dominant superconducting instability in this regime has p-wave symmetry. Upon decreasing the density of holes, λ increases gradually. Approaching the zero hole density limit, λ increases sharply, and the dominant pairing channel changes to d wave. λ diverges in the limit $n_e \to 0$, due to the diverging density of states [33].

Kohn-Luttinger mechanism in RTG.—Turning to RTG, we use a realistic model for the band structure and $\Lambda_{\boldsymbol{k},\boldsymbol{q},\tau}$ [33]. The resulting FSs of the inner and outer pockets in Fig. 1(e) show a substantial trigonal warping, leading to anisotropic $\Pi_{0,\boldsymbol{q}}$. However, some of the features are similar to those of the circularly symmetric model. λ as a function of density [Fig. 1(g)] is qualitatively similar to that of the circularly symmetric model, showing a sharp increase at the density where the inner pocket appears ($n_e \approx -2.1 \times 10^{12}$ cm^{-2}), followed by a gradual increase of λ with decreasing hole density. The symmetry of the order parameter changes from extended s wave (A_1 representation of the point group C_{3v} of RTG with a perpendicular electric field), with an opposite sign on the inner and outer Fermi pockets, to p wave (representation E). λ diverges logarithmically at the Van Hove density $n_e \approx -0.5 \times 10^{12}$ cm^{-2}, where the annulus reconstructs into three disconnected pockets. Focusing on the p-wave phase and going beyond the linearized gap equation, the favored state below T_c is a chiral $p_x + ip_y$ state, which can be derived by considering the quartic terms in the Ginzburg-Landau free energy functional [33].

Importantly, in Eq (1), spin singlet and triplet pairing are degenerate, independently of the orbital symmetry of the order parameter. This counterintuitive result follows from the SU(2) × SU(2) symmetry of the Hamiltonian, which allows us to rotate the spin of one valley relative to the other [30,35,36]. In the singlet (triplet) case, the order parameter in valley $\tau = +1$ has the same (opposite) phase to that of valley -1, such that the Pauli principle is obeyed. We shall discuss the lifting of the singlet-triplet degeneracy below.

Figures 2(a),2(b) show the density and Δ_1 dependence of λ in the spin and valley unpolarized phase [$N = 4$ in Eq. (3)], corresponding to the SC1 region in experiment [16]. Increasing Δ_1 shifts the peak corresponding to the van Hove singularity (VHS) towards charge neutrality. However, there is a broad density regime ($n_e < -0.8 \times 10^{12}$ cm^{-2}) where λ is an increasing function of Δ_1 at a fixed density, following the trend of the density of states with Δ_1 in this regime. This is consistent with the fact that the SC1 phase is entered upon increasing electric field in the unpolarized phase [16]. To account for $T_c = 0.1$ K in SC1, assuming that $W \approx E_F \approx 50$ K, we need $\lambda \approx 0.16$. As seen in Fig. 2, our theory can produce λ's of this order. In the vicinity of the VHS, λ diverges logarithmically, and our theory breaks down. The VHS are not attained in experiment, since they are preceded by Stoner transitions [15]. We note

that the dispersion features a higher order VHS at $\Delta_1 \approx 18$ meV [33,37].

Figures 2(c),2(d) show λ as a function of density and Δ_1 assuming a spin polarized, valley-unpolarized state ($N = 2$), which corresponds to the experimentally observed normal state of SC2 [15,16,38]. The overall trends are similar to those of Figs. 2(a),2(b), although for a spin-polarized normal state, the pairing is necessarily spin triplet. The magnitude of λ is somewhat larger than for $N = 4$, due to stronger effective interaction [Eq. (3)]. This is in apparent disagreement with experiment. We speculate that the reason for this discrepancy is the residual Hund's coupling, not considered in Eq. (1), which may favor spin singlet pairing (see below).

Finally, in Fig. 3 we show the dependence of λ on the dielectric constant ϵ and the distance to the gates d for three values of the electron density. λ increases with decreasing ϵ, since superconductivity originates from repulsive interactions. Interestingly, λ is nearly independent of d for $d \gtrsim 4$ nm because the pairing benefits primarily from large momentum scattering processes where q is of the order of $2k_F$ [39].

Role of the Hund's coupling.—The lifting of the degeneracy between between singlet and triplet pairing requires an intervalley interaction that depends on the relative spin of the two electrons. Such an interaction is short ranged in real space, and receives contributions from the short-range part of the Coulomb interaction and from electron-phonon coupling [40,41]. The simplest term of this form is an intervalley Hund's coupling, $H_{\text{Hund}} = -J_H \int d^2 r \boldsymbol{S}_+ \cdot \boldsymbol{S}_-$, where $\boldsymbol{S}_\pm$ are the spin densities in the two valleys. J_H may be of either sign.

In general, $J_H > 0$ ($J_H < 0$) favors triplet (singlet) pairing, respectively. However, for, e.g., a $p_x + ip_y$ state, H_{Hund} drops out of the linearized gap equation (4) and does not lift the singlet-triplet degeneracy [33]. Physically, this is because H_{Hund} is local in real space, and nonzero angular momentum of $p_x + ip_y$ leads to vanishing amplitude of the two electrons to be at the same location.

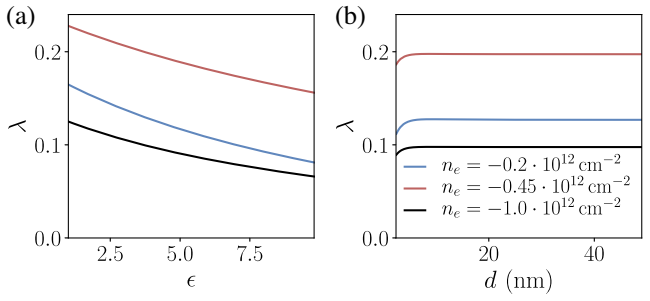

FIG. 3. λ as a function of dielectric constant ϵ (a) and distance to the gate d (b). The results are for $\Delta_1 = 20$ meV and densities listed in the legend correspond to the three pocket FS (blue), two annular FS near VHS (red), and the regime of annulus away from the singularity (black).

To lift the degeneracy in the $p_x + ip_y$ state, one needs to go beyond the assumption of a momentum independent (i.e., local) Hund's term. We assume that the effective Hund's coupling depends on distance, $J_H(\boldsymbol{r} - \boldsymbol{r}')$. Expanding its Fourier transform $\tilde{J}_H$ at small momenta as $\tilde{J}_H(\boldsymbol{q}) = J_{H,0} + J_{H,2}(qa)^2 + O(q^4)$ (where a is the graphene lattice spacing), we find that $J_{H,2} > 0$ ($J_{H,2} < 0$) favors singlet (triplet) pairing [33]. Hence, the lifting of the degeneracy is determined by the sign of the residual nonlocal Hund's coupling, which can be of either sign relative to $J_{H,0}$, depending on microscopic details. $J_{H,2} > 0$ corresponds to a negative second moment of $J_H(\boldsymbol{r})$, i.e., the effective Hund's coupling is *antiferromagnetic* in some range of distances, which promotes singlet pairing.

Deriving the effective Hund's term microscopically is notoriously difficult [41]. Instead, we can determine the signs of $J_{H,0}$ and $J_{H,2}$ from the experiment. We assume that $J_{H,0} > 0$, favoring ferromagnetism, and $J_{H,2} > 0$, favoring singlet pairing in the $p_x + ip_y$ phase. Hence, the SC1 phase, which emerges out of a spin-unpolarized normal state, is spin singlet. Note that for a simple s-wave order parameter (with no sign change of $\Delta_{\boldsymbol{k}}$ within a single valley), the leading-order $J_{H,0}$ term is sufficient to lift the singlet-triplet degeneracy. Hence, $J_{H,0} > 0$ (required by the presence of valley-unpolarized ferromagnets) implies that SC1—if it were simple s wave—should be spin triplet, in contradiction with experiment.

The normal state of SC2 is a fully spin polarized ferromagnet, and hence SC2 must be spin triplet, which is consistent with the strong violation of the Pauli limit in SC2 seen in experiment. In our model, the spin triplet state is disfavored by $J_{H,2} > 0$, which can potentially explain the fact that T_c of SC2 is substantially lower than that of SC1 [16]. That being said, we emphasize that for SC2, spin triplet pairing is still much favored over spin singlet, because there are no opposite spins to pair with at the Fermi energy.

Discussion.—We demonstrated that repulsive interactions can give rise to robust unconventional superconductivity in two-dimensional systems with annular FSs that are similar to RTG in the parameter regimes where superconductivity was recently discovered. The Kohn-Luttinger mechanism is consistent with the absence of a strong temperature dependence of the resistivity above T_c and can further explain the apparent discrepancy between SC1 being spin singlet and the presence of a nearby spin polarized phase, implying that the intervalley exchange coupling is ferromagnetic.

An outstanding question is whether the superconducting state in RTG is indeed unconventional. In contrast to s-wave pairing [42,43], unconventional SC is very sensitive to non-magnetic disorder [44–47]. Thus, introducing controlled amounts of disorder to the system could be used to identify the nature of the superconducting state [48]. Another prediction of our theory is the near degeneracy

between singlet and triplet pairing, which is also expected within an electron-phonon mechanism [30]. As SC1 is suppressed by an in-plane field, a triplet state may be stabilized at lower temperature. So far, T_c of SC1 was found to be suppressed below 50 mK with the application of an in-plane field [16], but a triplet SC with a lower T_c is possible. Furthermore, a fully spin polarized SC2 is expected to have exotic properties, due to the intertwining of the SC phase with the orientation of the magnetization [49]. The most likely pairing state within our theory is a chiral $p_x + ip_y$ SC that breaks time reversal symmetry and generates spontaneous edge currents [50–52]. Since within the symmetry group of RTG p-wave and d-wave pairings are not distinct from each other, the obtained pairing is reminiscent of the spin-singlet chiral d-wave pairing predicted for doped graphene [53–58].

The pairing mechanism proposed in this work is mediated by electronic fluctuations with a broad spectrum, and does not assume the existence of a soft collective mode at low energies (that arises if the system is close to a continuous phase transition). If such a soft mode exists, it could enhance T_c further. Very recent studies of this scenario [59,60] found a chiral p-wave state similar to our work.

Finally, it is desirable to raise T_c in RTG and other systems with annular FSs. Our theory predicts a significant enhancement of λ near the VHS where the inner and outer FSs meet. In RTG, the metallic state becomes unstable towards spin or valley polarization before this point is reached. We speculate that decreasing distance to metallic gates d may suppress these instabilities, while not affecting superconductivity significantly until $d \approx 4$ nm (Fig. 3), effectively enhancing SC phase.

We thank Yang-Zhi Chou, Andrey Chubukov, Johannes Hofmann, Steve Kivelson, Sri Raghu, and Sankar das Sarma, Jay Sau, Fengcheng Wu, and Andrea Young for many stimulating discussions and for their comments on the manuscript. E. B. thanks S. Chatterjee, T. Wang, and M. Zaletel for a collaboration on a related topic. A. G. acknowledges support by the European Union's Horizon 2020 research and innovation program under the Marie Sklodowska-Curie Grant Agreement No. 754411. E. B. and T. H. were supported by the European Research Council (ERC) under grant HQMAT (Grant Agreement No. 817799), by the Israel-USA Binational Science Foundation (BSF), and by a Research grant from Irving and Cherna Moskowitz.

[*] A. G. and T. H. contributed equally to this work.

[1] B. E. Feldman, J. Martin, and A. Yacoby, Broken-symmetry states and divergent resistance in suspended bilayer graphene, Nat. Phys. **5**, 889 (2009).

[2] A. S. Mayorov, D. C. Elias, M. Mucha-Kruczynski, R. V. Gorbachev, T. Tudorovskiy, A. Zhukov, S. V. Morozov, M. I. Katsnelson, A. K. Geim, and K. S. Novoselov, Interaction-driven spectrum reconstruction in bilayer graphene, Science **333**, 860 (2011).

[3] Y. Cao, V. Fatemi, A. Demir, S. Fang, S. L. Tomarken, J. Y. Luo, J. D. Sanchez-Yamagishi, K. Watanabe, T. Taniguchi, E. Kaxiras *et al.*, Correlated insulator behaviour at half-filling in magic-angle graphene superlattices, Nature (London) **556**, 80 (2018).

[4] Y. Cao, V. Fatemi, S. Fang, K. Watanabe, T. Taniguchi, E. Kaxiras, and P. Jarillo-Herrero, Unconventional superconductivity in magic-angle graphene superlattices, Nature (London) **556**, 43 (2018).

[5] X. Lu, P. Stepanov, W. Yang, M. Xie, M. A. Aamir, I. Das, C. Urgell, K. Watanabe, T. Taniguchi, G. Zhang *et al.*, Superconductors, orbital magnets and correlated states in magic-angle bilayer graphene, Nature (London) **574**, 653 (2019).

[6] X. Liu, Z. Hao, E. Khalaf, J. Y. Lee, Y. Ronen, H. Yoo, D. H. Najafabadi, K. Watanabe, T. Taniguchi, A. Vishwanath *et al.*, Tunable spin-polarized correlated states in twisted double bilayer graphene, Nature (London) **583**, 221 (2020).

[7] M. Yankowitz, S. Chen, H. Polshyn, Y. Zhang, K. Watanabe, T. Taniguchi, D. Graf, A. F. Young, and C. R. Dean, Tuning superconductivity in twisted bilayer graphene, Science **363**, 1059 (2019).

[8] G. Chen, A. L. Sharpe, P. Gallagher, I. T. Rosen, E. J. Fox, L. Jiang, B. Lyu, H. Li, K. Watanabe, T. Taniguchi *et al.*, Signatures of tunable superconductivity in a trilayer graphene moiré superlattice, Nature (London) **572**, 215 (2019).

[9] Z. Hao, A. Zimmerman, P. Ledwith, E. Khalaf, D. H. Najafabadi, K. Watanabe, T. Taniguchi, A. Vishwanath, and P. Kim, Electric field–tunable superconductivity in alternating-twist magic-angle trilayer graphene, Science **371**, 1133 (2021).

[10] J. M. Park, Y. Cao, K. Watanabe, T. Taniguchi, and P. Jarillo-Herrero, Tunable strongly coupled superconductivity in magic-angle twisted trilayer graphene, Nature (London) **590**, 249 (2021).

[11] M. Koshino and E. McCann, Trigonal warping and berry's phase $n\pi$ in ABC-stacked multilayer graphene, Phys. Rev. B **80**, 165409 (2009).

[12] F. Zhang, B. Sahu, H. Min, and A. H. MacDonald, Band structure of ABC-stacked graphene trilayers, Phys. Rev. B **82**, 035409 (2010).

[13] M. Koshino, Interlayer screening effect in graphene multilayers with ABA and ABC stacking, Phys. Rev. B **81**, 125304 (2010).

[14] K. F. Mak, J. Shan, and T. F. Heinz, Electronic Structure of Few-Layer Graphene: Experimental Demonstration of Strong Dependence on Stacking Sequence, Phys. Rev. Lett. 2010) 176404 ,**104**).

[15] H. Zhou, T. Xie, A. Ghazaryan, T. Holder, J. R. Ehrets, E. M. Spanton, T. Taniguchi, K. Watanabe, E. Berg, M. Serbyn, and A. F. Young, Half and quarter metals in rhombohedral trilayer graphene, Nature (London) **598**, 429 (2021).

[16] H. Zhou, T. Xie, T. Taniguchi, K. Watanabe, and A. F. Young, Superconductivity in rhombohedral trilayer graphene, Nature (London) **598**, 434 (2021).

[17] For a related mechanism for unconventional superconductivity in trilayer graphene, starting from the Hubbard model,

see H. Dai, J. Hou, X. Zhang, Y. Liang, and T. Ma, Mott insulating state and $d+id$ superconductivity in an ABC graphene trilayer, Phys. Rev. B **104**, 035104 (2021).
[18] W. Kohn and J. M. Luttinger, New Mechanism for Superconductivity, Phys. Rev. Lett. **15**, 524 (1965).
[19] M. Y. Kagan, V. A. Mitskan, and M. M. Korovushkin, Anomalous superconductivity and superfluidity in repulsive fermion systems, Phys. Usp. **58**, 733 (2015).
[20] S. Raghu, S. A. Kivelson, and D. J. Scalapino, Superconductivity in the repulsive Hubbard model: An asymptotically exact weak-coupling solution, Phys. Rev. B **81**, 224505 (2010).
[21] S. Maiti and A. V. Chubukov, Superconductivity from repulsive interaction, AIP Conf. Proc. **1550**, 3 (2013).
[22] Similarly, a two-dimensional band structure with multiple sub-bands has been predicted to be favorable for an unconventional mechanism for superconductivity [23,24].
[23] S. Raghu and S. A. Kivelson, Superconductivity from repulsive interactions in the two-dimensional electron gas, Phys. Rev. B **83**, 094518 (2011).
[24] A. V. Chubukov and S. A. Kivelson, Superconductivity in engineered two-dimensional electron gases, Phys. Rev. B **96**, 174514 (2017).
[25] I. I. Mazin, D. J. Singh, M. D. Johannes, and M. H. Du, Unconventional Superconductivity with a Sign Reversal in the Order Parameter of $LaFeAsO_{1-x}F_x$, Phys. Rev. Lett. **101**, 057003 (2008).
[26] U. Zondiner, A. Rozen, D. Rodan-Legrain, Y. Cao, R. Queiroz, T. Taniguchi, K. Watanabe, Y. Oreg, F. von Oppen, A. Stern, E. Berg, P. Jarillo-Herrero, and S. Ilani, Cascade of phase transitions and Dirac revivals in magic-angle graphene, Nature (London) **582**, 203 (2020).
[27] D. Wong, K. P. Nuckolls, M. Oh, B. Lian, Y. Xie, S. Jeon, K. Watanabe, T. Taniguchi, B. A. Bernevig, and A. Yazdani, Cascade of electronic transitions in magic-angle twisted bilayer graphene, Nature (London) **582**, 198 (2020).
[28] A. M. Clogston, Upper Limit for the Critical Field in Hard Superconductors, Phys. Rev. Lett. **9**, 266 (1962).
[29] B. S. Chandrasekhar, A note on the maximum critical field of high-field superconductors, Appl. Phys. Lett. **1**, 7 (1962).
[30] Y.-Z. Chou, F. Wu, J. D. Sau, and S. D. Sarma, Acoustic-Phonon-Mediated Superconductivity in Rhombohedral Trilayer Graphene, Phys. Rev. Lett. **127**, 187001 (2021).
[31] P. B. Allen, The electron-phonon coupling constant, *Handbook of Superconductivity*, edited by Charles P. Poole, Jr. (Academic Press, San Diego, 2000), Ch. 9 Sec. G, p. 478, 10.1016/B978-012561460-3/50010-2.
[32] A possible resolution is that that J_H changes its sign as a function of density. However, since J_H is a lattice-scale interaction, it seems unlikely it changes significantly upon a small change in electron concentration.
[33] See Supplemental Material at http://link.aps.org/supplemental/10.1103/PhysRevLett.127.247001 for more details on the band structure and polarization function of RTG and the circularly symmetric model, the method for calculation of T_c, the SC state below T_c, and the Hund's coupling.
[34] A. V. Chubukov, Kohn-Luttinger effect and the instability of a two-dimensional repulsive Fermi liquid at $T=0$, Phys. Rev. B **48**, 1097 (1993).
[35] J. Y. Lee, E. Khalaf, S. Liu, X. Liu, Z. Hao, P. Kim, and A. Vishwanath, Theory of correlated insulating behaviour and spin-triplet superconductivity in twisted double bilayer graphene, Nat. Commun. **10**, 5333 (2019).
[36] E. Khalaf, P. Ledwith, and A. Vishwanath, Symmetry constraints on superconductivity in twisted bilayer graphene: Fractional vortices, $4e$ condensates or non-unitary pairing, arXiv:2012.05915.
[37] N. F. Q. Yuan, H. Isobe, and L. Fu, Magic of high-order van Hove singularity, Nat. Commun. **10**, 5769 (2019).
[38] We note that due to the trigonal warping in RTG, in a each valley, $\varepsilon_{\boldsymbol{k},\tau} \neq \varepsilon_{-\boldsymbol{k},\tau}$, and hence a valley-polarized state does not have a BCS instability.
[39] In the case where the FS is composed of disjoint pockets, $2k_F$ should replaced by the maximum distance between points on the FS.
[40] J. Alicea and M. P. A. Fisher, Graphene integer quantum Hall effect in the ferromagnetic and paramagnetic regimes, Phys. Rev. B **74**, 075422 (2006).
[41] M. Kharitonov, Phase diagram for the $\nu=0$ quantum Hall state in monolayer graphene, Phys. Rev. B **85**, 155439 (2012).
[42] P. W. Anderson, Theory of dirty superconductors, J. Phys. Chem. Solids **11**, 26 (1959).
[43] A. M. Finkel'stein, Suppression of superconductivity in homogeneously disordered systems, Physica (Amsterdam) **197B**, 636 (1994).
[44] A. A. Abrikosov and L. P. Gor'kov, Contribution to the theory of superconducting alloys with paramagnetic impurities, Zh. Eksp. Teor. Fiz. **39**, 1781 (1960) [Sov. Phys. JETP **12**, 1243 (1961)].
[45] P. I. Larkin, Vector pairing in superconductors of small dimensions, Zh. Eksp. Teor. Fiz. Pis'ma Red. **2**, 205 (1965) [Sov. Phys. JETP Lett. **2**, 130 (1965)].
[46] A. J. Millis, S. Sachdev, and C. M. Varma, Inelastic scattering and pair breaking in anisotropic and isotropic superconductors, Phys. Rev. B **37**, 4975 (1988).
[47] R. J. Radtke, K. Levin, H.-B. Schüttler, and M. R. Norman, Predictions for impurity-induced T_c suppression in the high-temperature superconductors, Phys. Rev. B **48**, 653 (1993).
[48] A. P. Mackenzie, R. K. W. Haselwimmer, A. W. Tyler, G. G. Lonzarich, Y. Mori, S. Nishizaki, and Y. Maeno, Extremely Strong Dependence of Superconductivity on Disorder in Sr_2RuO_4, Phys. Rev. Lett. **80**, 161 (1998).
[49] E. Cornfeld, M. S. Rudner, and E. Berg, Spin-polarized superconductivity: Order parameter topology, current dissipation, and multiple-period Josephson effect, Phys. Rev. Research **3**, 013051 (2021).
[50] A. Furusaki, M. Matsumoto, and M. Sigrist, Spontaneous Hall effect in a chiral p-wave superconductor, Phys. Rev. B **64**, 054514 (2001).
[51] M. Stone and R. Roy, Edge modes, edge currents, and gauge invariance in p_x+ip_y superfluids and superconductors, Phys. Rev. B **69**, 184511 (2004).
[52] J. A. Sauls, Surface states, edge currents, and the angular momentum of chiral p-wave superfluids, Phys. Rev. B **84**, 214509 (2011).

[53] Annica M. Black-Schaffer and Carsten Honerkamp, Chiral *d*-wave superconductivity in doped graphene, J. Phys. Condens. Matter **26**, 423201 (2014).

[54] Annica M. Black-Schaffer and Sebastian Doniach, Resonating valence bonds and mean-field *d*-wave superconductivity in graphite, Phys. Rev. B **75**, 134512 (2007).

[55] Wei Wu, Michael M. Scherer, Carsten Honerkamp, and Karyn Le Hur, Correlated Dirac particles and superconductivity on the honeycomb lattice, Phys. Rev. B **87**, 094521.

[56] Rahul Nandkishore, L. S. Levitov, and A. V. Chubukov, Chiral superconductivity from repulsive interactions in doped graphene, Nat. Phys. **8**, 158 (2012).

[57] Wan-Sheng Wang, Yuan-Yuan Xiang, Qiang-Hua Wang, Fa Wang, Fan Yang, and Dung-Hai Lee, Functional renormalization group and variational Monte Carlo studies of the electronic instabilities in graphene near 1 4 doping, Phys. Rev. B **85**, 035414 (2012).

[58] Maximilian L. Kiesel, Christian Platt, Werner Hanke, Dmitry A. Abanin, and Ronny Thomale, Competing many-body instabilities and unconventional superconductivity in graphene, Phys. Rev. B **86**, 020507(R) (2012).

[59] S. Chatterjee, T. Wang, E. Berg, and M. P. Zaletel, Inter-valley coherent order and isospin fluctuation mediated superconductivity in rhombohedral trilayer graphene, arXiv:2109.00002.

[60] Z. Dong and L. Levitov, Superconductivity in the vicinity of an isospin-polarized state in a cubic Dirac band, arXiv:2109.01133.